APPARENT WALL SLIP IN THE FULLY DEVELOPED LAMINAR FLOW OF VISCOPLASTIC LIQUIDS THROUGH TUBES

Paulo Roberto de Souza Mendes
José Roberto Ruschel Siffert
Eduardo Stein Soares Dutra
Pontifícia Universidade Católica - RJ
Rua Marquês de São Vicente 225, Rio de Janeiro - RJ 22453-900
pmendes@mec.puc-rio.br, jrsiffert@mec.puc-rio.br, essd@mec.puc-rio.br

Abstract. *We employ a recently proposed viscosity function (Souza Mendes and Dutra, 2004) to analyze the fully developed flow of yield-stress liquids through tubes. We first show that its dimensionless form gives rise to the so-called jump number, a novel material property that measures the shear rate jump that the material undergoes as the yield stress is reached. We integrate numerically the momentum conservation equation that governs this flow together with the generalized Newtonian Liquid model and the above mentioned viscosity function. We obtain velocity and viscosity profiles for the entire range of the jump number. We show that the friction factor $f.Re$ curves display sharp peaks as the shear stress value at the tube wall approaches the yield stress. Finally, we demonstrate the existence of sharp flow rate increases (or apparent slip) as the wall shear stress is increased in the vicinity of the yield stress.*

Keywords: *yield stress, wall slip, viscoplastic liquids, pressure drop, slurries, pastes, suspensions, emulsions*

1. Introduction

Flows of viscoplastic liquids are found in numerous industrial processes. In drilling and cementing operations of oil wells, are viscoplastic liquids both the drilling fluids and the cement slurries. In the food industry, mayonnaise, butter, ice cream are examples of viscoplastic liquids.

Until rather recently, these materials were modeled as if their viscosity were infinite at stress values below the yield stress. With the advent of extremely sensitive and accurate optical encoders, it has become possible to measure non-zero deformation rates of the order of 10^{-7}s^{-1}, which occur at stress values below the yield stress (Barnes, 1999; Roberts et al., 2001). In other words, the last-generation rheometers allowed the rheologists to unveil the very-high-viscosity Newtonian plateau that exists in the viscosity function of these viscoplastic liquids at stresses lower than the yield stress.

Recently Souza Mendes and Dutra (2004) proposed a four parameter viscosity function for viscoplastic liquids that describes accurately and in the whole range of shear stress (or rate) the recently discovered behavior of viscoplastic liquids. These authors also proposed a robust method for measuring the yield stress.

In this paper we revisit the laminar fully-developed flow of viscoplastic liquids in tubes to include the interesting transition that occurs when the wall shear stress value is in the vicinity of the yield stress. These features cannot be predicted with the classical viscosity functions, and are clearly related to the often observed and so far not fully understood phenomenon of wall slip.

2. Analysis

2.1 Momentum balance and constitutive hypothesis

For the fully developed flow through a tube of radius R, driven by an axial pressure gradient dp/dz, an overall force balance yields

$$\tau_R = -\frac{dp}{dz}\frac{R}{2} \tag{1}$$

where $\tau_R \equiv \tau(R)$ is the wall shear stress,

$$\tau \equiv \sqrt{\text{tr}\,\boldsymbol{\tau}^2/2}$$

being the intensity of the extra-stress tensor field $\boldsymbol{\tau}$. For this simple flow, of course $\tau = -\tau_{r\theta}$, where $\tau_{r\theta}$ is the $r\theta$ component of $\boldsymbol{\tau}$.

The momentum conservation principle also dictates that the shear stress $\tau_{r\theta}$ is a linear function of the radial coordinate r. We can thus write:

$$\tau = \tau_R\frac{r}{R} \tag{2}$$

Equations (1) and (2) must hold for the fully developed flow of all materials in tubes.

2.2 The dimensionless SMD equation and the jump number

In this paper we assume that the material behaves according to the following equation (Souza Mendes and Dutra, 2004), referred to in this text as the SMD equation for shortness:

$$\tau = \left(1 - \exp\left[-\frac{\eta_o \dot{\gamma}}{\tau_o}\right]\right)(\tau_o + K\dot{\gamma}^n) \tag{3}$$

In this equation, $\dot{\gamma} \equiv \sqrt{\mathrm{tr}\,\dot{\boldsymbol{\gamma}}^2/2}$ is the intensity of the rate-of-deformation tensor field, $\dot{\boldsymbol{\gamma}} \equiv \nabla \boldsymbol{u} + \nabla \boldsymbol{u}^T$, and $\boldsymbol{u}$ is the velocity vector field. For this flow, $\boldsymbol{u} = u(r)\hat{\boldsymbol{e}}_z$, and

$$\dot{\gamma} = -\dot{\gamma}_{r\theta} = -\frac{du}{dr} \tag{4}$$

The parameters that appear in Eq. (3), namely, η_o, τ_o K, and n, are respectively the low shear rate viscosity, the yield stress, the consistency index, and the behavior or power-law index. The physical meaning of these material parameters is discussed in detail by Souza Mendes and Dutra (2004).

It is interesting to note from the SMD equation that, when the stress τ reaches the yield stress τ_o, there is a sharp increase of the shear rate with no appreciable change in stress, i.e. the shear stress remains roughly equal to τ_o while the shear rate value jumps from a value around $\dot{\gamma}_o$ to an often much larger value in the vicinity of $\dot{\gamma}_1$, where

$$\dot{\gamma}_o \equiv \frac{\tau_o}{\eta_o}; \quad \dot{\gamma}_1 \equiv \left(\frac{\tau_o}{K}\right)^{1/n} \tag{5}$$

We can now define the **jump number** J, which gives a relative measure of the shear rate jump that occurs at $\tau = \tau_o$:

$$J \equiv \frac{\dot{\gamma}_1 - \dot{\gamma}_o}{\dot{\gamma}_o} = \frac{\eta_o \tau_o^{\frac{1-n}{n}}}{K^{1/n}} - 1 = \frac{\dot{\gamma}_1}{\dot{\gamma}_o} - 1 = \frac{1 - \dot{\gamma}_o^*}{\dot{\gamma}_o^*} \tag{6}$$

It is worth emphasizing that the jump number is a dimensionless rheological property of a given viscoplastic liquid.

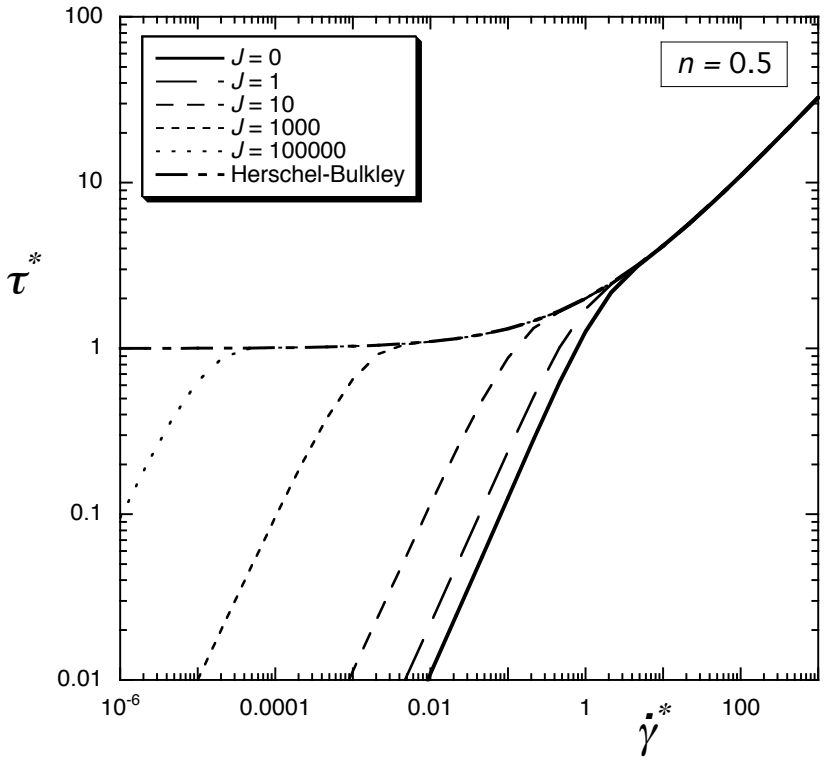

Figure 1. The dimensionless SMD shear stress function.

Choosing $\dot{\gamma}_1$ as characteristic shear rate and τ_o as the characteristic shear stress, so that $\tau^* \equiv \tau/\tau_o$ and $\dot{\gamma}^* \equiv \dot{\gamma}/\dot{\gamma}_1$ are respectively the dimensionless versions of the shear stress and shear rate, then we can write the following dimensionless form of Eq. (3):

$$\tau^* = (1 - \exp\left[-(J+1)\dot{\gamma}^*\right])(1 + \dot{\gamma}^{*n}) \tag{7}$$

This function is shown for $n = 0.5$ in Fig. 1, for the full range of jump numbers $0 \leq J < \infty$. When $J = 0$, there is no shear rate jump, and the SMD equation becomes suitable to represent shear-thinning, Carreau-type liquids. As $J \to \infty$, the SMD equation approaches the Herschel-Bulkley equation.

The viscosity function η is defined as $\eta \equiv \tau/\dot{\gamma}$. Accordingly, the dimensionless viscosity function is given by

$$\eta^* = \frac{\tau^*}{\dot{\gamma}^*} = \frac{\eta}{\eta_o}(J+1) = (1 - \exp\left[-(J+1)\dot{\gamma}^*\right]) \left(\frac{1}{\dot{\gamma}^*} + \dot{\gamma}^{*n-1}\right) \tag{8}$$

3. Method of solution

The dimensionless versions of Eqs. (2) and (4) are respectively

$$\tau^* = \tau_R^* r^* \tag{9}$$

and

$$\dot{\gamma}^* = -\frac{du^*}{dr*} \tag{10}$$

where $u^* \equiv u/\dot{\gamma}_1 R$ is the dimensionless axial velocity. Combining Eqs. (7) and (9), we get

$$\tau_R^* r^* = (1 - \exp\left[-(J+1)\dot{\gamma}^*\right])\,(1 + \dot{\gamma}^{*n}) \tag{11}$$

We then combine Eqs. (10) and (11) to obtain an ordinary differential equation for the velocity profile $u^*(r^*)$. The problem is solved numerically with the aid of a uniform mesh of 100 nodal points along the radial coordinate r. This mesh was shown to yield mesh-independent results for all cases investigated. To handle the non-linear nature of this equation, for each set of values of the parameters $\{\tau_R^*, J, n\}$, the following solution strategy is adopted:

1. for each nodal point, we solve Eq. (11) iteratively for $\dot{\gamma}$;
2. we then integrate Eq. (10) using finite-differences, using the axial symmetry and no-slip boundary conditions, namely, $\dot{\gamma}^*(0) = 0$ and $u^*(1) = 0$.

4. Results and discussion

We now present and discuss the results obtained in the form of velocity and viscosity profiles. We also discuss the influence of the wall shear stress τ_R^* on both the average axial velocity $\bar{u}^*$, obtained from

$$\bar{u}^* = 2\int_0^1 u^* r^* dr^* \tag{12}$$

and the product $f.Re$ of the friction factor $f \equiv -4(dp/dz)R/\rho\bar{u}^2$ with the Reynolds number $2\rho\bar{u}R/\eta_R$, where ρ is the mass density, $\dot{\gamma}_R \equiv \dot{\gamma}(R)$, and $\eta_R = \eta(\dot{\gamma}_R)$. The expression for $f.Re$ becomes

$$\frac{f.Re}{64} = \frac{\dot{\gamma}_R^*}{4\bar{u}^*} \tag{13}$$

Figure 2 illustrates the shape of the axial velocity profile as a function of J, n, and τ_R^*. It is seen from the first two graphs ($\tau_R^* = 10$) that, for wall shear stress values much larger than the yield stress, the jump number has essentially no effect on the profile shape, which is the one obtained with the classical Ostwald-de Waele (power-law) model. However, as illustrated in the graphs pertaining to τ_R^* values closer to unity, the jump number dictates the shape of the velocity profile, especially at larger values of the power-law index n.

The viscosity profiles shown in Fig. 3 illustrate the dramatic viscosity changes that occur for high jump numbers in the vicinity of the radial position where the shear stress equals the yield stress. When this radial position is close to the tube wall, a thin layer of low-viscosity, lubricating liquid is observed, yielding the steep wall velocity gradients observed in Fig. 2.

The product $f.Re$ is shown in the graphs of Fig. 4 as a function of the wall shear stress τ_R^*. It is firstly observed that for $\tau_R^* << 1$ the Newtonian result $f.Re = 64$ is obtained, because in this range of stress the liquid is Newtonian with a viscosity equal to η_o (or else, $\eta^* = J+1$). In the other extreme of $\tau_R^* >> 1$, the power-law result $f.Re = 64(3n+1)/4n$ is obtained, because the unyielded region in the neighborhood of the tube axis in this case becomes very small, not affecting the wall velocity gradient. In the range $0.1 < \tau_R^* < 10$, however, the jump number has a striking effect on $f.Re$, especially for larger values of n. The maximum peak value expected is $f.Re_{\max} = 64(J+1)$, which corresponds to the case of discontinuous derivatives at $\dot{\gamma}^* = \dot{\gamma}_o^*$ and $\dot{\gamma}^* = 1$ (bi-viscosity model, Beverly and Tanner (1992), see Fig. 1).

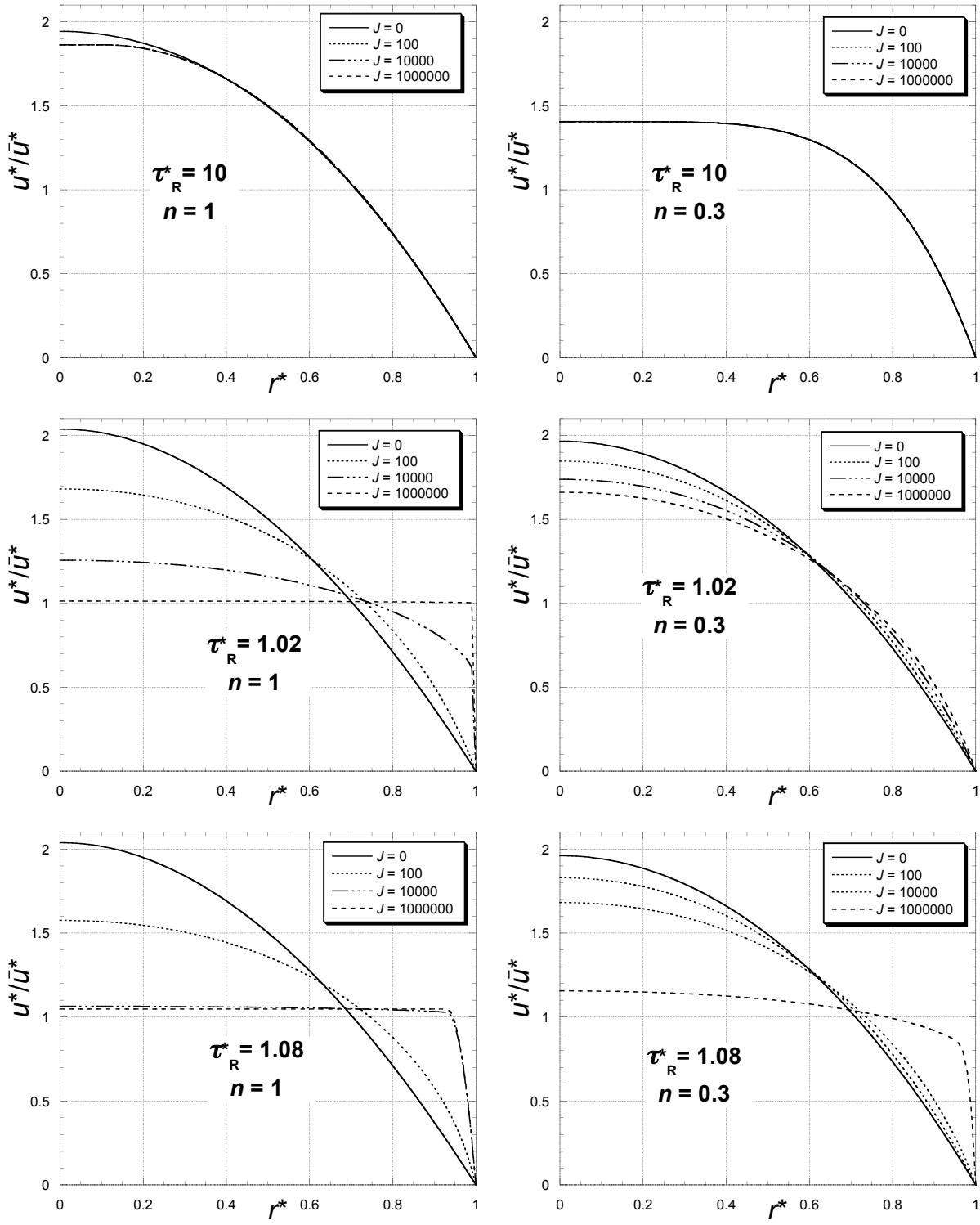

Figure 2. Dimensionless velocity profiles.

Because the SMD equation has continuous derivative throughout the $\dot{\gamma}^*$ range, the transitions at $\dot{\gamma}^* = \dot{\gamma}_o^*$ and $\dot{\gamma}^* = 1$ are smooth and hence the peak values are smaller and smoother. The actual shape of the bumps depends directly on the shape of the corresponding $\tau^* \times \dot{\gamma}_o^*$ curve in Fig. 1.

The peak values of $f.Re$ occur as $\tau_R^* \to 1$ and when the shear rate jumps up but the thickness of the low-viscosity layer is still negligibly small. As τ_R^* is increased further, but still in the neighborhood of $\tau_R^* = 1$, this thickness departs from zero and hence the average velocity undergoes a steep increase, which causes $f.Re$ to decrease (see Eq. (13)). As τ_R^* is increased even further, the $f.Re$ value approaches asymptotically its power-law value.

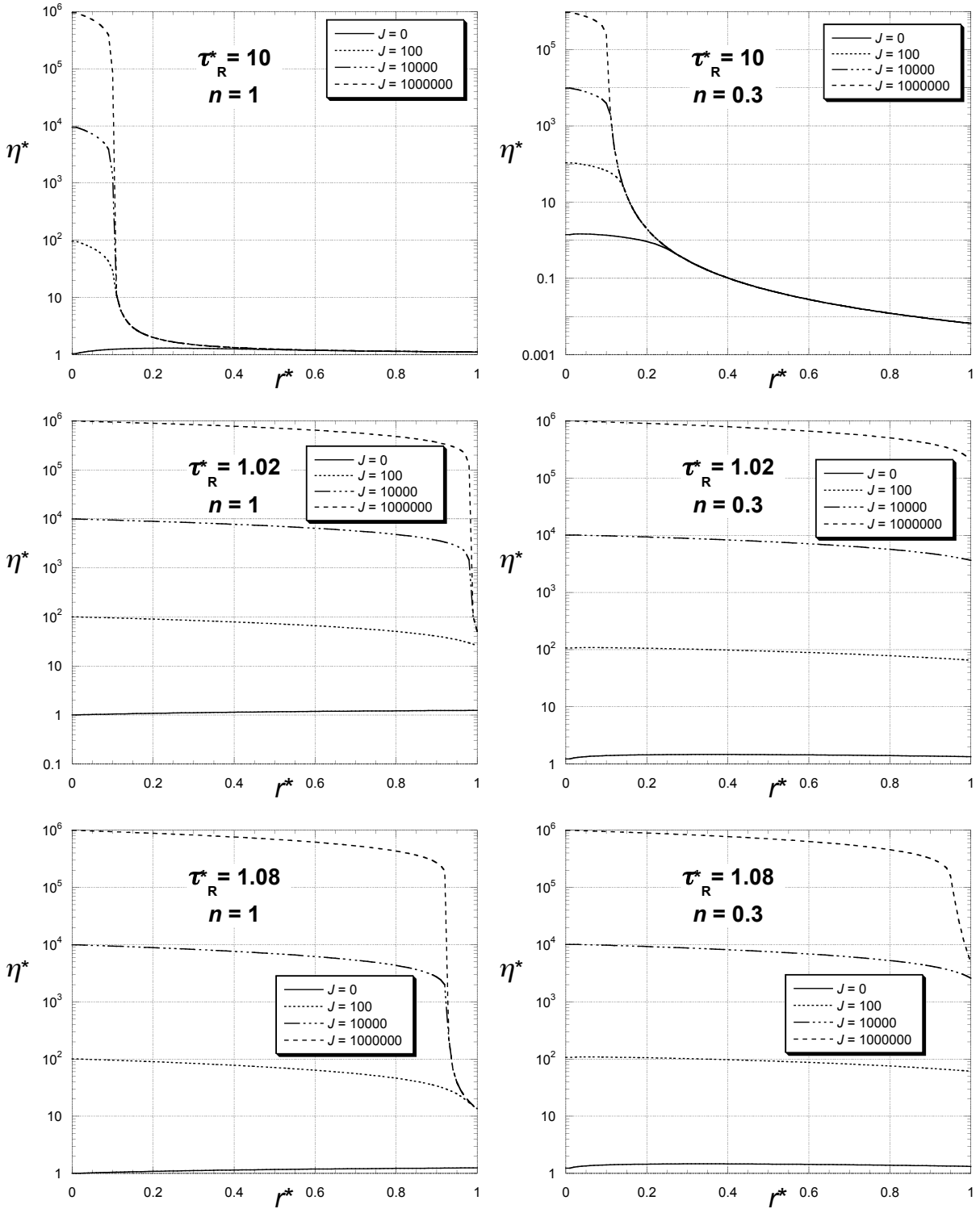

Figure 3. Dimensionless viscosity profiles.

Figure 5 shows the dimensionless average velocity as a function of the dimensionless wall shear stress for different values of the jump number. A sharp flow rate increase is observed for high jump number values just beyond $\tau_R^* = 1$. It is seen that the dimensionless velocity jumps up by a factor roughly equal to the jump number value, that is

$$\bar{u}^{*+} \simeq J\bar{u}^{*-} \tag{14}$$

where $\bar{u}^{*-}$ and $\bar{u}^{*+}$ are the values of the dimensionless average velocity for wall shear stress values just below and just above the yield stress, respectively.

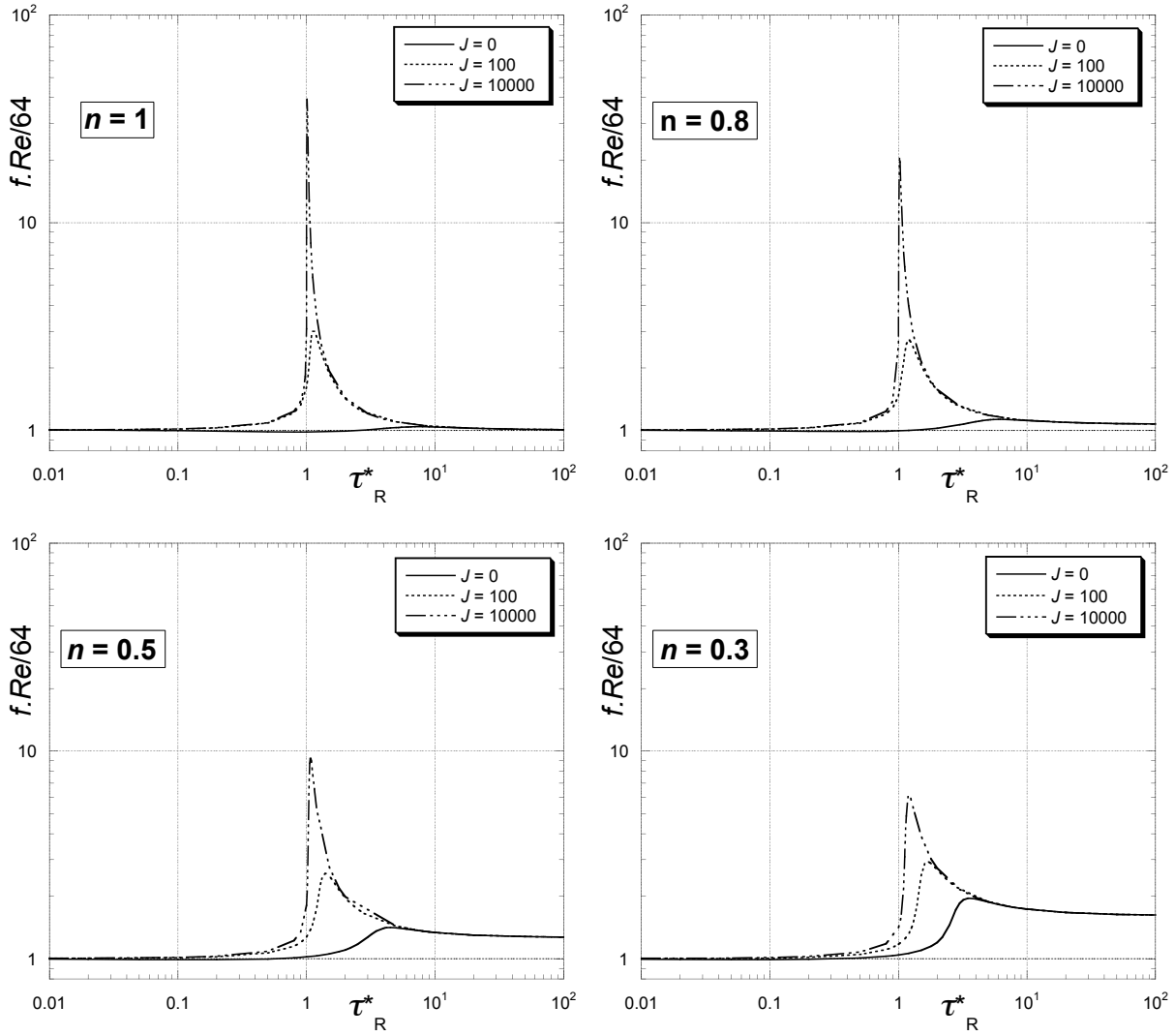

Figure 4. Friction factor as a function of the dimensionless wall shear stress.

5. Conclusions

We have employed the SMD viscosity function to analyze the fully developed flow of yield-stress liquids through tubes. We have first introduced the concept of jump number, a novel material property that gives a relative measure of the shear rate jump that the material undergoes as the yield stress is reached. We have integrated numerically the momentum conservation and constitutive equations to obtain velocity and viscosity profiles for the entire range of the jump number. When the wall shear stress is slightly larger than the yield stress, a thin low-viscosity layer at the wall is formed, which causes steep velocity gradients., If observed experimentally, the flow under these conditions could give the erroneous appearance of the occurrence of wall slip. Finally, we have shown that the friction factor $f.Re$ curves display sharp peaks as the shear stress value at the tube wall approaches the yield stress.

6. Acknowledgements

The authors are indebted to Petrobras S.A., CNPq, CAPES, FAPERJ, FINEP, and MCT for the financial support to the Group of Rheology at PUC-RIO.

7. References

Barnes, H. A., 1999. The yield stress – a review. J. Non-Newt. Fluid Mech. 81, 133–178.

Beverly, C. R., Tanner, R. I., 1992. Numerical analysis of three-dimensional Bingham plastic flow. J. Non-Newtonian Fluid Mechanics 42, 85–115.

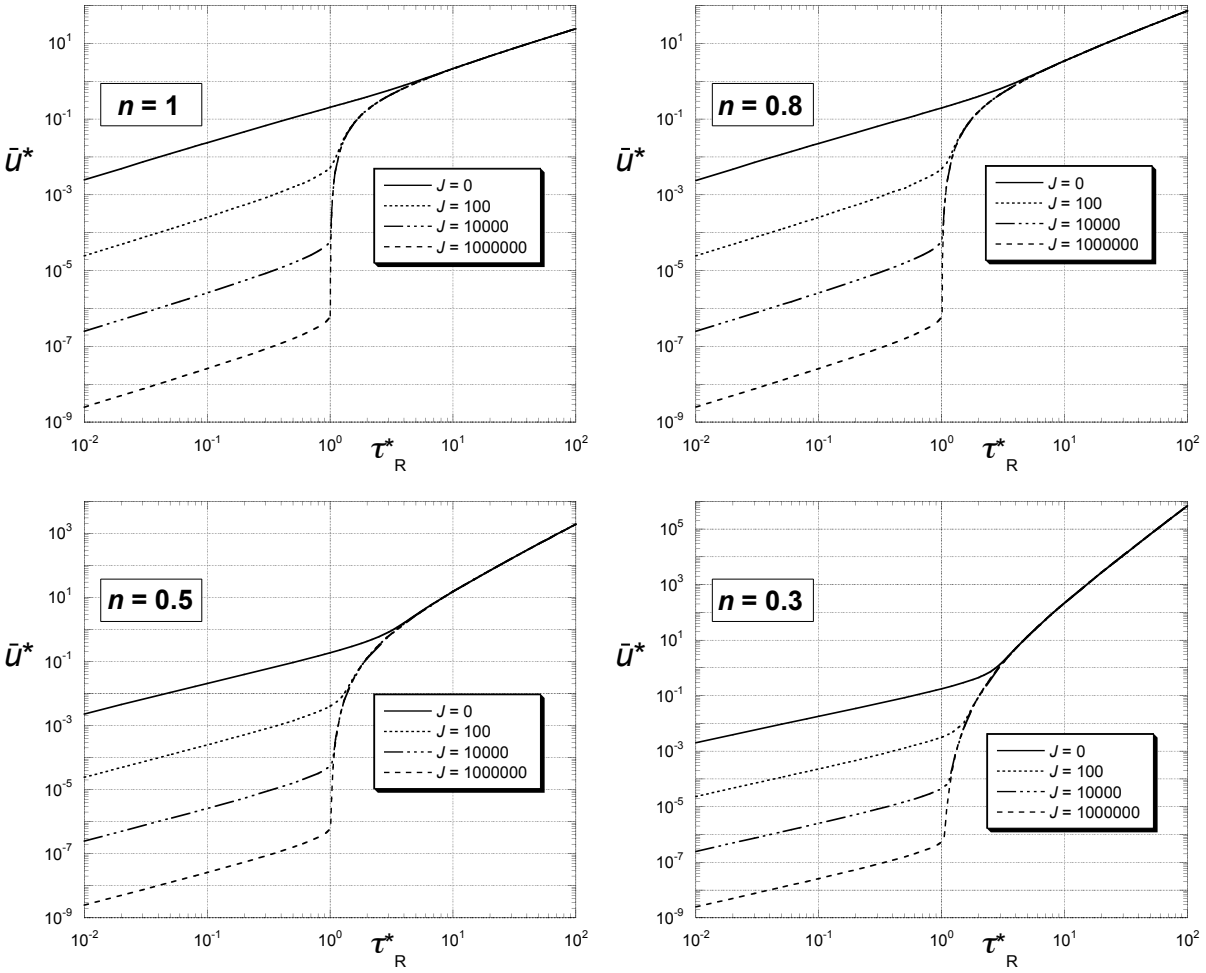

Figure 5. Dimensionless average velocity as a function of the dimensionless wall shear stress.

Roberts, G. P., Barnes, H. A., Carew, P., 2001. Modelling the flow behaviour of very shear-thinning liquids. Chemical Engineering Science 56, 5617–5623.

Souza Mendes, P. R., Dutra, E. S. S., 2004. Viscosity function for yield-stress liquids. Applied Rheology 14 (6), 296–302.

8. Responsibility notice

The author(s) is (are) the only responsible for the printed material included in this paper